

## Mechanisms of cluster implantation in silicon: A molecular-dynamics study

Sigeo Ihara and Satoshi Itoh

Central Research Laboratory, Hitachi Ltd., Kokubunji, Tokyo 185-8601, Japan

Jun'ichi Kitakami

Hitachi ULSI Engineering Corporation, Kokubunji, Tokyo 185-0014, Japan

(Received 24 March 1998)

Employing molecular dynamics, we have simulated collisions of various sizes of 5.7-keV silicon clusters with a silicon surface. At this energy, the simulation provides an atomistic description of the evolution of the multiple scattering process of atoms in the cluster as well as the substrate where atoms interact with each other by covalent forces. The change from the collision cascade that is characteristic in the single-ion case to the simultaneous collision process that leads to the collective motion of particles, such as macroscopic vibration of the surface and shock waves, is found by increasing the number of the atoms in the cluster. With an increase in cluster size, the impurity profile and the damaged region for the cluster ion implantation is also found to be shallower. In contrast to single-ion implantation, cluster implantation may not induce defects in deep regions, making it suitable for device design. The channeling effect is found to be mainly suppressed by the low-frequency macroscopic vibrations of the surface rather than by the amorphization of the surface caused by the impact. [S0163-1829(98)03136-1]

### I. INTRODUCTION

In order to create low-leakage junctions for future high-speed and scaled down device structures, low-energy implantation is necessary for the preparation of very shallow junctions, constituting the source-channel and drain-channel regions of metal-oxide-semiconductor (MOS) devices. For example, ultrashallow doping with depth less than scores in nm is required for sub-0.1- $\mu\text{m}$  metal-oxide-semiconductor field-effect transistors (MOSFET's).<sup>1</sup> In making such shallow junctions with a high concentration of impurities, the depth of the defects from the surface should be much shallower to suppress transient enhanced diffusion (TED),<sup>2</sup> which is caused by the excess point defects in the region of implant damage. The above requirement extends the ion implantation technique towards lower energies of keV order. However, standard ion-implantation technology, such as  $\text{B}^+$  implantation, results in problems such as the inherent channeling effect, anomalous diffusion due to damage such as TED, lateral diffusion under the mask, and so on.<sup>3</sup>

Using molecules or clusters for the ion source is one promising solution<sup>4</sup> since such sources reduce the effective energy per constituting atom more than what could be achieved by lowering the accelerating voltage of the ion implanter.<sup>5</sup> Recently,  $\text{BF}_2^+$  has been used to make shallow junctions, although it suffers from a boron penetration problem caused by the existence of fluorine.<sup>6</sup> Seeking a lower-energy and higher-dosage boron ion implantation technique, Goto *et al.*<sup>7</sup> used the decaborane molecule,  $\text{B}_{10}\text{H}_{14}$ , with a plus charge as an implanted ionized particle. Since  $\text{B}_{10}\text{H}_{14}^+$  contains ten boron atoms, it can be implanted with about a one-tenth lower effective acceleration energy and a ten times higher effective beam current when compared with  $\text{B}^+$ . (The impact energy of the hydrogen atoms are ignored because their masses are much smaller than those of boron.) Takeuchi *et al.*<sup>8</sup> showed experimentally that the boron secondary ion mass spectroscopy (SIMS) profile of the boron cluster,

decaborane  $\text{B}_{10}\text{H}_{14}$ , implanted into a Si(100) surface at 20 keV is quite similar to that of  $\text{B}^+$  implanted at 2 keV. Moreover, implanted boron atoms are electrically activated, which is desirable in boron implantation. Nevertheless, they reported that there is an inherent channeling effect,<sup>8</sup> although the suppression of the channeling effect is dramatic. Takeuchi conjectured that the suppression of the channeling effect by using a cluster ion is due to the amorphization of the silicon substrate crystal induced by the cluster impact. However, neither the collision mechanism that results from the impact of clusters on a Si(100) surface, nor their influence on the types or number of induced defects are clear, despite past work on the surface impact of clusters.<sup>9</sup> The purpose of this work is to study these issues in the context of the cluster impact mechanism.

In keV implantation where nuclear stopping is dominant compared with the electronic stopping (this is the converse of the high-energy implantation process),<sup>10</sup> the single-ion implantation process can be described as follows. When an energetic ion collides with an atom in a crystal lattice with enough energy, the lattice atom will collide with other lattice atoms, resulting in a large number of successive collisions. All atomic collisions initiated by a single ion are called a cascade.

Molecular dynamics<sup>11,12</sup> is a useful tool for investigating the collision phenomena in keV energy regimes, where the multiple scattering, i.e., more than two atoms colliding with each other simultaneously, and the many-body interaction between atoms becomes important, because the time evolutions of many atoms (i.e., positions and velocities) are obtained simultaneously without assuming a specific collision mechanism. This is in contrast to the often-used Monte Carlo simulation method for implantation, such as TRIM (Ref. 13) and MARLOWE.<sup>14</sup> In these simulations, a binary collision mechanism where two particles collide with each other by pairwise interaction is assumed.<sup>9</sup> As far as the single-ion implantation process is concerned, this collision mechanism

dominates in creating the collision cascade in the high-energy regime ( $> 10$  keV). Therefore its applicability to the low-energy implantation is not assured, since other mechanisms such as multiple scattering, which cannot be described by a binary collision mechanism, are expected to play an important role.<sup>15</sup> Because collision mechanism in general can be derived from the Newtonian mechanics (i.e., time evolution) of a system composed of particles, molecular dynamics has been used to study particle impact phenomena<sup>11,12</sup> from their early applications.

In recent work, Díaz de la Rubia and Gilmer<sup>16</sup> studied the single-ion (Si) implantation of 5 keV on a Si(100) surface using molecular dynamics employing three-body Stillinger-Weber potential<sup>17</sup> as well as a Langevin dynamics procedure. They showed that the primary knock-on atom mechanism is dominant in such a case. Although an amorphous region created by a 5-keV primary knock-on atom contains a thousand displaced atoms, only a few isolated Frenkel pairs remain, which finally collapse into clusters of interstitials or vacancies after 1 ns annealing at 1300 K. They also suggested that these defect clusters are primarily responsible for the enhanced diffusion of dopant atoms commonly observed in low-energy ion implanted silicon. These views are consistent with experimental results.<sup>18–21</sup>

Cluster impact on the surface has been studied using molecular dynamics by many researchers,<sup>9,22–24</sup> including fullerene C<sub>60</sub> clusters implanted on a graphite surface,<sup>9</sup> silicon cluster soft landing on a Si(100) surface,<sup>24</sup> and Ar cluster bombardment on a Si(100).<sup>22,23</sup> Gilmer and Roland<sup>24</sup> performed a three-dimensional simulation of the impact of 50 silicon clusters with energy 0.5 keV onto a Si (100) surface to investigate the film deposition process. Insepov and Yamada<sup>22</sup> calculated the depth profile of an Ar<sub>*n*</sub> (*n*=55–200) cluster ion with an energy of 10–100 eV/cluster in a two-dimensional surface. However, to our knowledge, the silicon cluster impact problem for Si(100) with an energy of about 5 keV that is characteristic of that used to implant dopants for shallow junctions in semiconductor devices has not been pursued.

In this work, by referring to the work of Díaz de la Rubia and Gilmer<sup>16</sup> for single ion implantation, we took a similar approach for simulating the cluster implantation process on a Si (100) surface. In particular, we have simulated collisions of approximately 5.7 keV using silicon clusters on a Si (100) surface with varying cluster sizes and temperatures. The aim of our work is to study the changes in the implantation process when clusters containing up to 90 atoms are used relative to single atoms (or ions) in the energy range of 5 keV.

## II. METHOD OF SIMULATION

In our molecular-dynamics simulations, the Stillinger-Weber potential was used to calculate forces between atoms, especially the covalent forces in silicon. The computational cell ( $16.053 \times 16.053 \times 36$  nm) contains 108 000 Si atoms and incident cluster, where the base of the cell is a square 16.053 nm on an edge and the height is 8 nm (with 28-nm vacuum region). As an initial position of atoms in the substrate, we prepare the truncated ideal silicon surface, i.e., we choose a perfect diamond structure as an initial position with the (100) surface at the top. Maxwellian velocity distribution

was chosen for the starting velocities of particles. The periodic boundary conditions were applied in all directions, but the atoms at the bottom two layers were held fixed in their initial position and all other atoms were allowed to move freely. In our calculation, the microcanonical (*EVN*) ensemble molecular-dynamics method with time reversible leapfrog time integration was used, where the total energy of the system *E*, volume *V*, and the number of particles *N* are chosen for the constant variables. In the process for obtaining thermal equilibrium state of the crystal using molecular dynamics, we obtained the reconstructed surface with dimers, which is the same as the dimerized surface previously obtained using the Stillinger-Weber potential.

The number of atoms in the incident cluster, *N<sub>c</sub>*, were chosen as 1, 8, 20, and 90. Hereafter we use the term “cluster” to refer to both a cluster with more than one atom and a single-atom (ion) case. For each cluster, the incident total kinetic energy is 5.7 keV. In most cases in our simulations for *N<sub>c</sub>*=1–90, atoms in the cluster have only translational velocity perpendicular to the surface; our modeling implies that all particles in a cluster have the same velocity proportion to square root of the total kinetic energy of cluster over *N<sub>c</sub>*. This does not allow the thermal fluctuation of particles in an incident cluster, thus corresponding to the situation in which the internal state has the same phonon state, or low temperature. However, this restriction was relaxed for the some simulations for *N<sub>c</sub>*=20. In these cases, the cluster’s center of mass has only translational velocity, but particles inside the cluster can have a different velocity by the following two methods: (1) cluster atoms have the rotational momentum around the *z* axis with energy corresponds to 3000 K, and (2) the velocities of atoms are completely random with energy corresponds to 4000 K.

Because at keV energies the electronic slowing down does not significantly contribute to the production of lattice defects, defect production is caused mainly by nuclear stopping, i.e., the collision between an incident ion and atoms in the substrate and the collision between substrate atoms. Here, we only take into account the effect of nuclear stopping using molecular dynamics. Because the time of the impact is too short, the impact phenomena may not strongly depend on the detailed interaction potential between incident and substrate particles. However, it is known that, in the keV regime, the simultaneous motion of particles is strongly affected by the presence of the many-body forces. Therefore, we choose the silicon cluster as an incident cluster ion impacting on a Si(100) surface for the sake of simplicity. Also, since the mass of the implanted element and the substrate are the same, the momentum transfer from atoms in the cluster to atoms in the substrate is maximally estimated in our case.

We have assumed that the incident cluster ion neutralizes before impact and therefore we can use the potentials for neutral species rather than ions. Hereafter we use the term “ions” to refer to the fast impacting neutral species as in Ref. 25. In our molecular-dynamics simulations, we changed the time step of the time integral according to the velocity of the fastest particle motion in the phenomena. Our simulations were performed using a HITACHI SR2201 parallel supercomputer and mainframe systems.

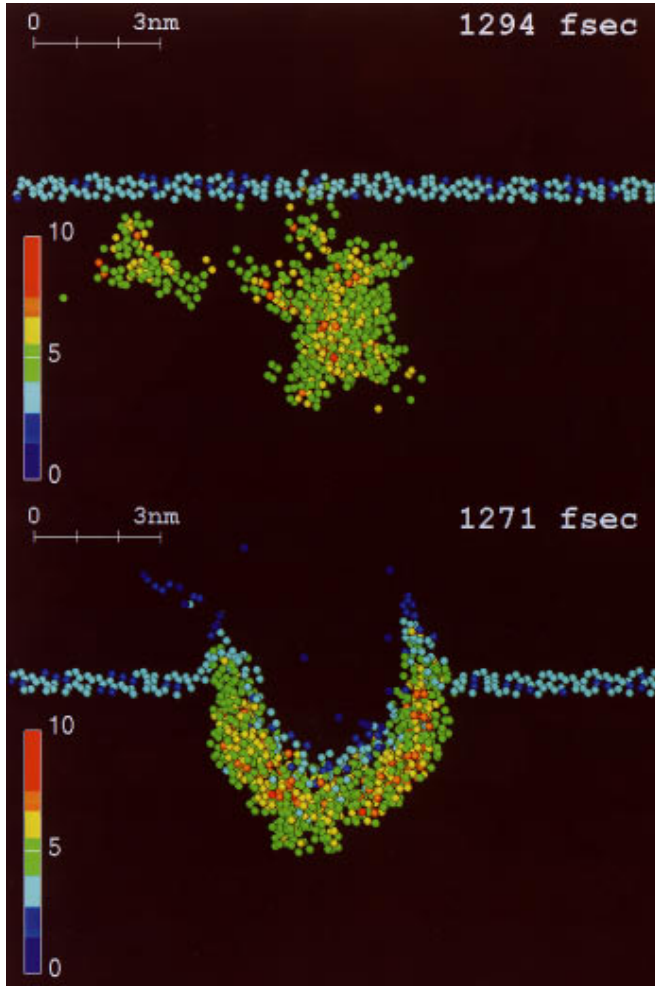


FIG. 1. (Color) The region damaged by a single (upper panel) and 90-atom cluster (lower panel) impacts both with 5.7 keV. The snapshots were obtained by slicing central regions of the incident location.

### III. RESULTS AND DISCUSSIONS

The simulation results depicted by particle and field image are given in Figs. 1 and 2, respectively. Only atoms *not* having four coordinated atoms are depicted in Fig. 1 (and Fig. 3). The coordination number used here is defined as the number of atoms inside of the sphere with radius  $R_s$  centered at an atom. (Here  $R_s$  is set to 0.3 nm, which is close to the nearest-neighbor distance of atoms in the diamond structure of silicon.) Since a perfect crystal form of silicon is a diamond structure in which atoms are four coordinated, the deviation in the coordination number from four normally means a defect, even though a defect may occasionally be four coordinated. In the color map, atoms having “the coordination number” 1 (dark blue), 2 (blue), or 3 (sky blue) indicates that atoms are near vacancies, while 5 (green), 6 (yellow), or 7 (orange), and, to a lesser extent, 8 (red), indicates interstitials. By dividing the computational box into finer meshes each having  $0.229 \times 0.229 \times 0.193$  nm, the local *field* variable for the physical quantities is determined by smearing corresponding particle variables contained in a mesh. For instance, to determine the local temperature at mesh point  $\mathbf{R}_i$ ,  $T_i^{\text{loc}}$ , we have smeared out the kinetic energy for the particle inside the sphere of radius 0.3 nm centered at

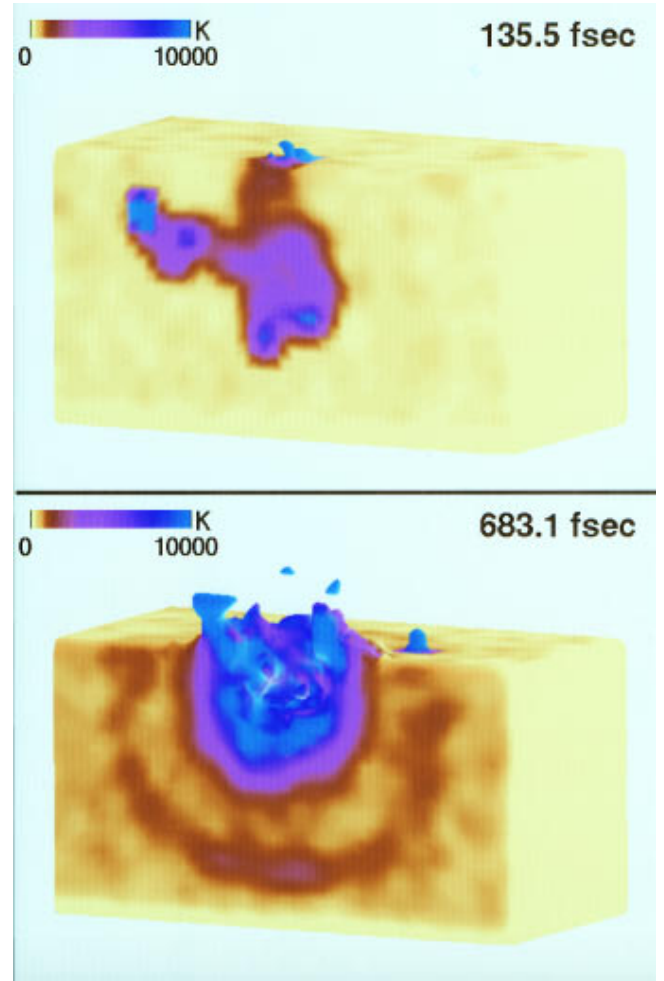


FIG. 2. (Color) The local temperature of damaged region for a single (upper panel) and 90-atom cluster (lower panel) impacts.

$\mathbf{R}_i$  and visualized, by the marching cubes method,<sup>26</sup>

$$T_i^{\text{loc}} = \frac{1}{6k_B N_i^{\text{loc}}} \sum_j^{N_i^{\text{loc}}} m_j v_j^2, \quad |\mathbf{r}_j - \mathbf{R}_i| < 0.3, \quad (3.1)$$

where  $\mathbf{R}_i$  is the mesh point,  $j$  indicates the index for the atom, and  $N_i^{\text{loc}}$  is the number of atoms in the local region around  $\mathbf{R}_i$ . Figures 2 and 4 show the cross-sectional view of the temperature field in the substrate. Similarly, the defect region is determined by the combination of the potential energy and bond analysis.

#### A. Single-ion case

Before going into detail regarding cluster implantation, single-ion implantation is discussed to clarify the changes in the physics of the impact. In some of the cases in our simulation, channeling was observed where the particle goes through the system within 0.1 ps, when an incident particle with 5.7 keV injected into the channeling sites. The temperature distribution obtained by smearing the particle velocity showed that the energy transfer of an atom to the substrate is very small, and thus causes no damage for the channeling case.

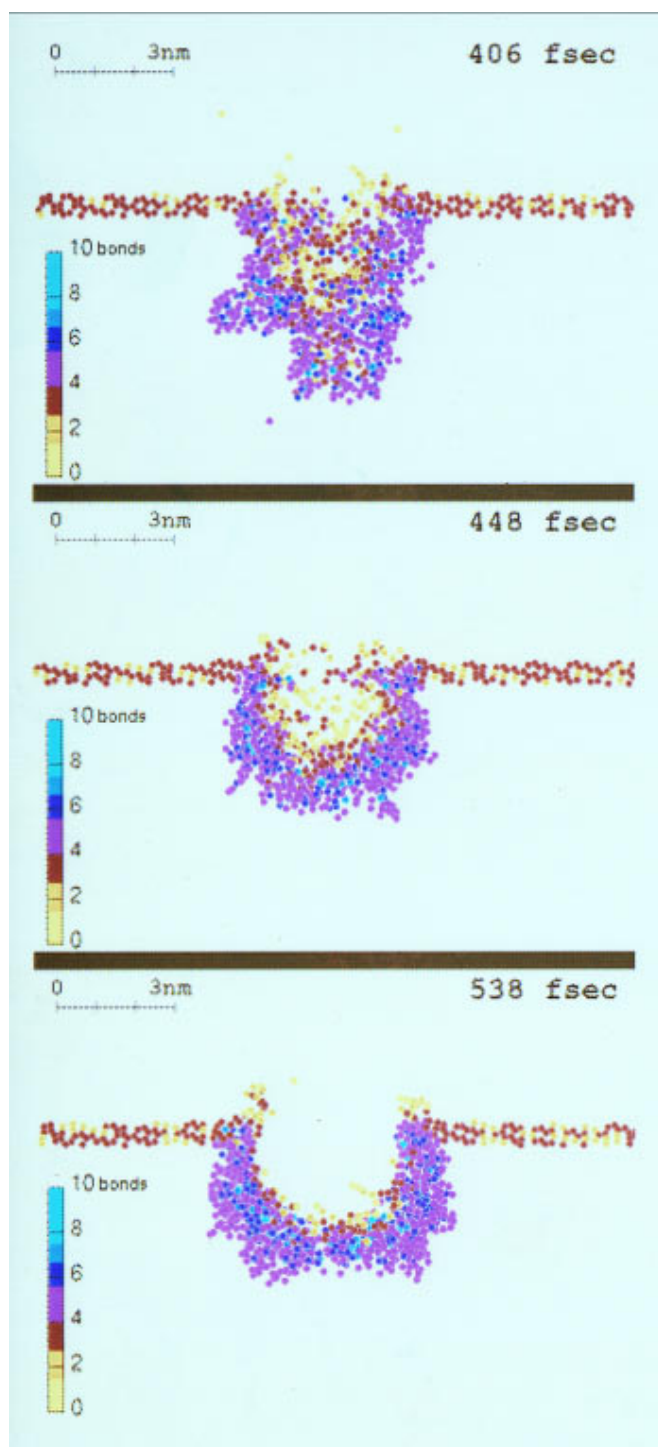


FIG. 3. (Color) The region damaged by  $N_c=8$  (upper panel),  $N_c=20$  (middle panel) and  $N_c=90$  (lower panel) cluster impacts with 5.7 keV. The snapshots were obtained by slicing central regions of the incident location.

The shallowest case for single-ion implantation without colliding with dimers is that in which the incident particle hit an atom in the third layer in the substrate and transferred its energy almost completely to it. The collision cascade for this case, which we will call  $N_c=1$  in our simulation, is depicted in Fig. 1 (upper). The impact is found to be localized and not symmetrical. There are many high-temperature regions in the early period after the collision (about 0.1–1 ps) that are

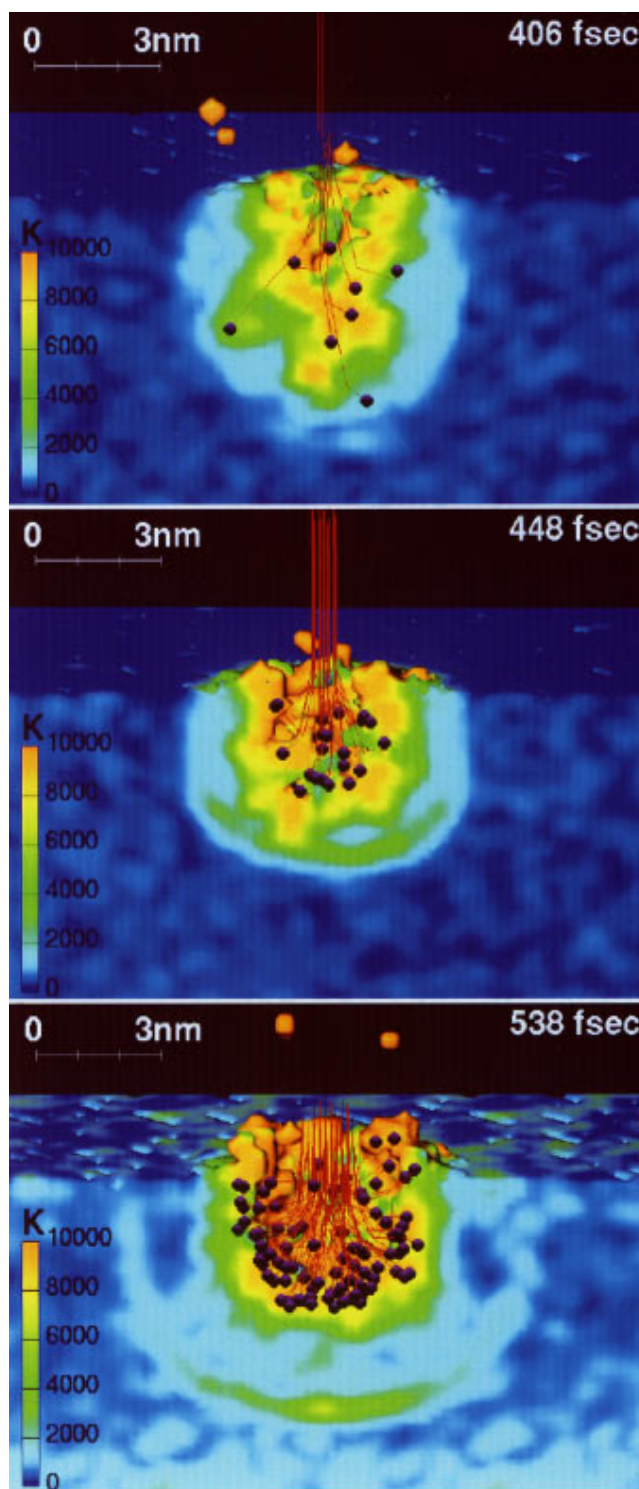


FIG. 4. (Color) The local temperature of the damaged region for cluster impacts at approximately 400 fs. From top to bottom, cluster sizes  $N_c=8$ , 20, and 90. Atoms in the cluster and their trajectories are depicted by purple balls and red lines, respectively.

spread [Fig. 2 (upper)] and reduced in the crystal by the heat conduction after 3 ps. The process of the dissipation of heat can be seen in the animation where the blinking light-blue spots increase. (The animation is available from the author.<sup>27</sup>) In this case, many defects induced in the crystal are finally recrystallized according to the annealing effect that results from the increasing temperature of the crystal. That

is, the energy transferred from the incident particle allows atoms to move to stable positions, thus allowing the damaged region to recover over time. Our results for single-ion implantation are consistent with previous studies such as that by Daiz de la Rubia and Gilmer.<sup>16</sup> The damaged region will recrystallize with only a small number of Frenkel pairs.

## B. Cluster implantation

### 1. Characteristic properties of cluster implantation

The most prominent difference between cluster impacts and those of a single ion is the global influence on the surface of the former. The damage caused by a cluster ion having the same kinetic energies for its constituent ions is isotropic, while that for the single-ion implantation is highly anisotropic (see Figs. 1 and 2). The process for generating damages in the cluster ion implantation, which takes several hundreds fs, is five to ten times slower than that in the single-ion case. In the single-ion case, a large number of successive collisions are induced in the deep region by the highly random knock-on atoms. In contrast, in the cluster impact case, the cross-sectional area of the cluster is larger so that the impact of a group of atoms with almost the same velocities will cause collective motion such as deformation or shock waves. These are clearly seen in Fig. 2 (lower) of the local temperature field representation of impact at 683 fs. The region in orange indicates that the temperature is higher than 20 000 K. In contrast to single-ion implantation, high-temperature regions (in orange) are well localized near the surface of the impact position, and turn into regions the temperatures of which are approximately 2500 K (in green) with time. Note that there are many orange spots distributed in the crystals well below the surface for single-ion implantation.

It is generally believed that the cluster size and inner state have a great influence on the number of defects and their distribution. In our simulation at 5.7 keV, the cluster breaks into isolated atoms after the impact since the impact energy far exceeds the cohesive energy of the crystal (4.6 eV/atom), but almost all atom in the cluster for all  $N_c$  are injected into the surface as can be seen in Fig. 2 (lower). This corresponds to the previous simulation results, where the cluster is destroyed completely below 10 keV, but only a small number of atoms are evaporated.<sup>20,21</sup> On the other hand, the ejection of substrate atoms from the surface occurs when cluster size is increased, with a rim forming around a crater. At  $N_c=20$  and 90, the ejection from the substrate becomes prominent, while at  $N_c=8$  (or less), such an effect is not substantial.

### 2. Effects in the substrate

The cluster impact produces a crater at a time of 0.4 ps after the cluster is injected. The crater is a result of the deformation of substrate materials (see Fig. 3). The deformed region expands quickly within 2.7 ps but it can not fill the crater for  $N_c=20$  and 90. In our simulations, there remains a dip for the  $N_c=20$  and 90 cases, although the compressed region of  $N_c=8$  recovered almost completely. Whether a dip is created or not according to the cluster size is mainly due to the difference in collision mechanisms, which are discussed later on, since the injected energies for  $N_c=8, 20,$  and 90 are the same.

The remaining dip in our  $N_c=20$  and 90 cases is in contrast to the 50 Si 0.5 keV/cluster impact into the Si(100) surface of Ref. 24, where the compressed region expands to fill the crater within 0.6 ps. This difference is, however, due to the impact energy: the greater the impact energy, the greater the degree of deformations.

To obtain a microscopic view, we performed an analysis (for  $N_c=20$  and 90) of the time dependence of the position of the atoms along the  $z$  axis just below the impact position and along the  $x$  axis parallel to the surface. After impact, atoms near the impact position exchange their sequence in positions for both measured directions, indicating that the deformation is plastic. While atoms are far below the surface or far from the impact region, they retain their position sequences, indicating that the deformation is elastic. This may explain the deformation nature of the crater. It is interesting to note that unlike a graphite surface,<sup>16</sup> the hump on the silicon surface is not prominent.

The dramatic phenomenon observed in a cluster impact is a shock wave.<sup>28</sup> For  $N_c=8$ , the shock wave propagation was not obvious in the study of the time evolution of the system as in our coloring picture. However, by increasing  $N_c$  (20 and 90), the shock waves having much higher temperature than melting point are clearly seen as a light-blue arc line in Figs. 2 and 4. An atomistic analysis clearly shows that this wave propagation does not induce defects, but rather merely propagates as a wave form in the substrate. The wave front is about 1 nm thick with a velocity along the  $z$  axis estimated from atomistic analysis to be 9 km/s, which agrees with the experimentally observed longitudinal sound velocity of 8.43 km/s.

The shock wave, for instance  $N_c=90$ , changes with time as follows. At 300 fs, a shock wave with  $T$  (temperature)  $>12\,000$  K occurs and loses its energy with multiple scattering. At 350 fs, a shock wave with high temperature ( $2000\text{ K} < T < 8000\text{ K}$ ) and with a thickness of about 1 nm wave front propagates. The occurrence of the shock wave, which is not responsible for forming defects in the deep layers of the crystals, is important to dissipate the impact energy. We have confirmed that the wave front of the shock wave is almost spherical, which is similar to the recently observed atomic laser pulse in solids performed by Mewes *et al.*,<sup>29</sup> where phonons are condensed into the Bose-Einstein condensation. In this case, the atomic laser emits millimeter-scale pulses of atoms, all propagating as a single wave. It has been shown that the position of the shock front as a function of time obeys the self-similarity form:  $R=At^\alpha$ , where  $R$  is the distance traveled by the shock wave in time  $t$  and the experimental value is  $\alpha=0.61$ . Our simulation provides  $\alpha=0.4$ , which does not agree with experiment. This may be due to the fact that our calculation time (and space) scale is rather too small to provide the asymptotic form.

### 3. Impurity atoms and the induced defects

As can be seen in Figs. 5 and 6, the impurity atoms (or injected atoms) in the case for  $N_c=8$  go deeper, reaching 4.7 nm, which is very close to 5.0 nm, the deepest depth of the defect generated by the impact for  $N_c=8$ . This value of the depth of defect is very close to the that of  $N_c=1$  case, 5.8 nm. This indicates that the depth profile of  $N_c=8$  is similar to that of  $N_c=1$ . However, the impurity atoms for  $N_c=20$

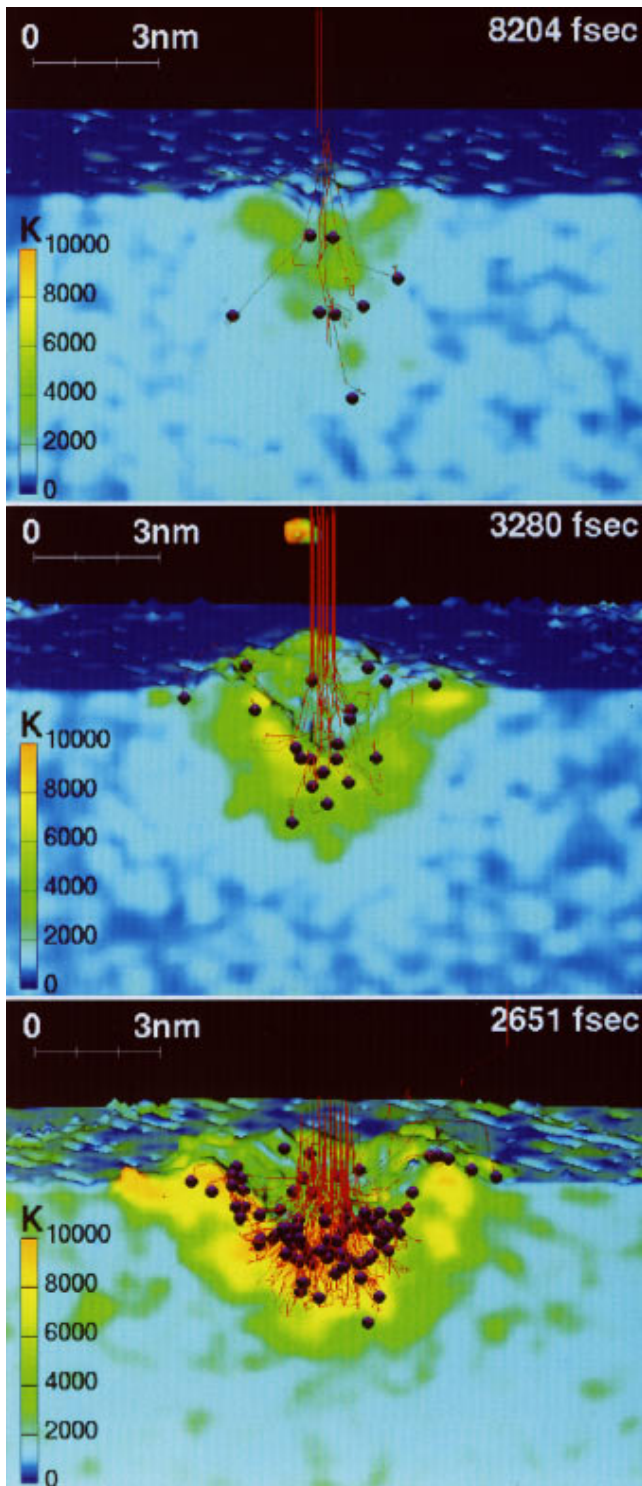


FIG. 5. (Color) The local temperature of the damaged region for cluster impacts over 3000 fs. From top to bottom, cluster sizes  $N_c = 8, 20,$  and  $90$ . Atoms in the cluster and their trajectories are depicted by purple balls and red lines, respectively.

and  $90$  cannot go deeper than  $2.9$  nm and  $3.0$  nm, respectively. Note that the depth of the deepest defect for  $N_c = 8, 20,$  and  $90$  is  $5.0, 3.9,$  and  $3.8$  nm, respectively. This shallowness of the impurity atoms arises from the fact that, as discussed later, if the impurity atoms even once go deeper, they are forced to move up by the environment. The macroscopic expansion (or vibrations) of the deformed region (to

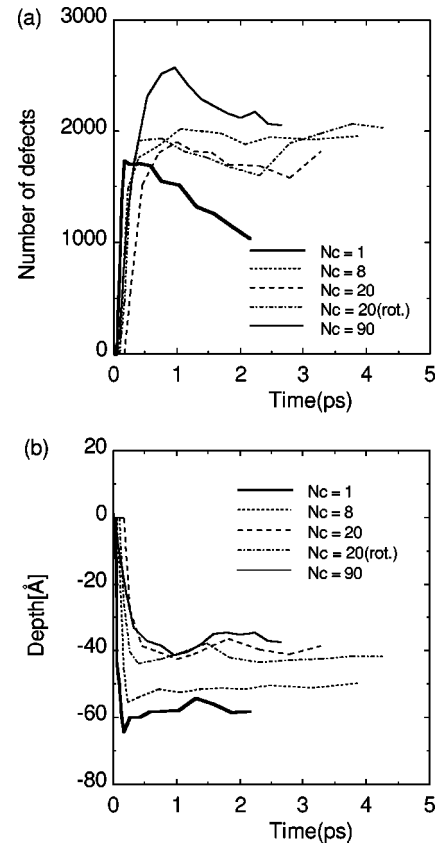


FIG. 6. Time dependence of the number of defects induced by collisions (a) and the depth of the deepest defect (b).

fill the crater) caused by the impact shifts the impurity atoms upwards. The degree of macroscopic expansion of the deformed region increase with increasing  $N_c$ . This can be clearly seen in the trajectories of the injected atoms shown in Figs. 4, 5, and 7, where the trajectories forms loops or arcs. This indicates that the impurity atoms do once go deeper, but that they change direction during  $2.7$  ps and move upward.

The time dependencies of the number of defects and the depth of the deepest defects induced by the impact for  $N_c = 1, 8, 20,$  and  $90$  are shown in Figs. 6(a) and 6(b), respectively. The bumps in the curves within  $3$  ps in Fig. 6(b) also indicates that the macroscopic expansion of the deformed region occurs. Note that  $N_c = 1$  corresponds to the implantation without channeling and the shallowest case. Figure 6(a) shows that the number of defects increases with  $N_c$  but decreases with time, while Fig. 6(b) shows that the defect positions become shallower with increasing  $N_c$ . (Note that in the  $N_c = 1$  case, the depth of the deepest defects is  $5.8$  nm.) Thus, this indicates that cluster implantation is suitable for making shallower junctions since no defects are induced in the deeper region, and the defects near the surface will be removed by the successive process after the implantation.

From the distribution of the coordination number in the thermal spike at  $3$  ps, the defect type in the thermal spike of the cluster impact differs from that of a single-ion impact. The defect types in the thermal spike for the different cluster sizes, however, will meet after annealing. For the single-ion case, how deep the collision cascade occurs, or whether channeling occurs or not, strongly depends on the impact position. However, for the cluster impact case, the difference

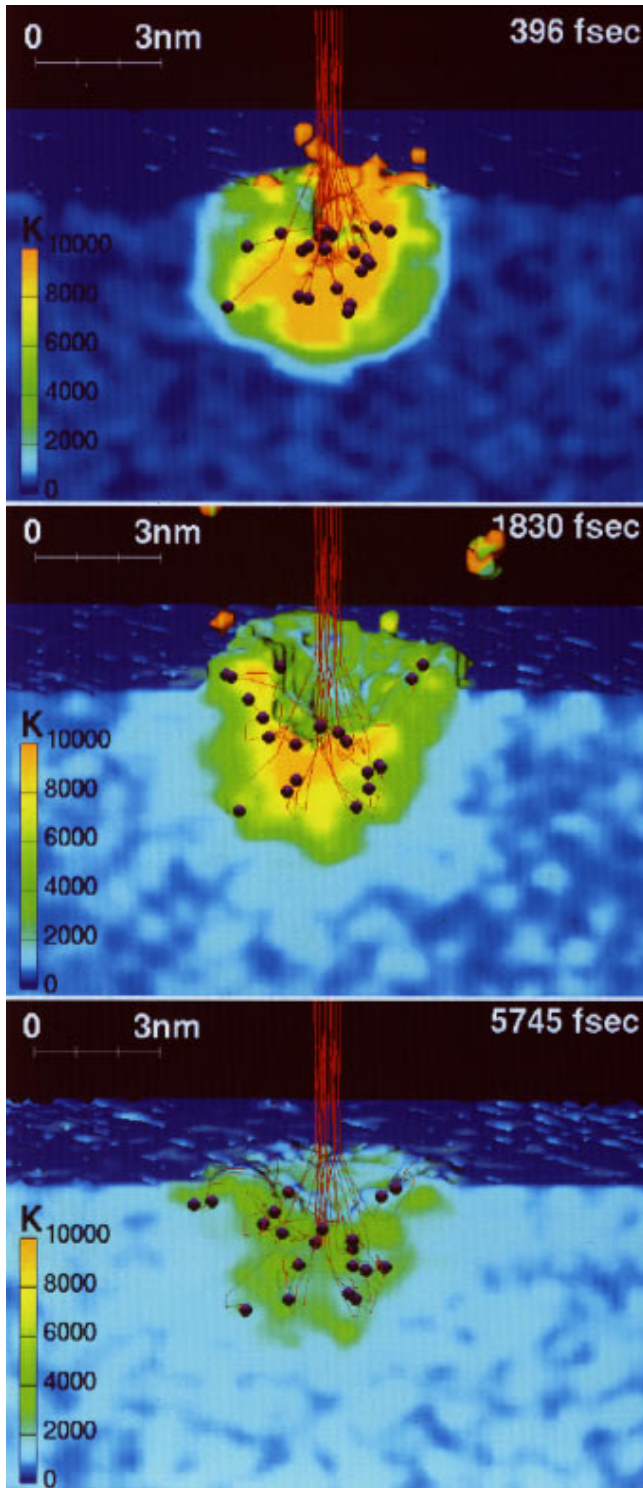


FIG. 7. (Color) The local temperature of the damaged region for  $N_c=20$  cluster impacts. From top to bottom, the time after collision is 396, 1830, and 5745 fs. Atoms in the cluster and their trajectories are depicted by purple balls and red lines, respectively.

in the individual impact may not be substantial, because the atoms in the cluster simultaneously interact with the substrate atoms in a wide area of the substrate.

Time-dependent analysis of the defect types that can be classified by the coordination number, or the bond number,  $n_b$  of defects was also performed. The impact for  $N_c=1-90$  with defects of  $n_b=5$  and 6 is dominant for every time

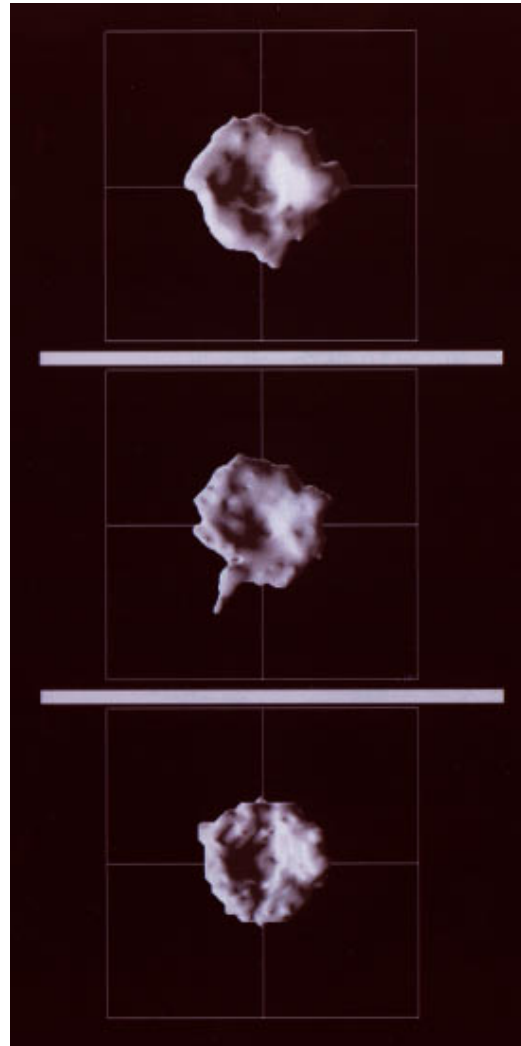


FIG. 8. (Color) Top view of the local temperature of damaged region for 20-atom cluster impacts for different interstates: uniform velocity (upper panel), rotation around the incident velocity (middle panel), and random velocity (lower panel).

in each case. The number of  $n_b=5$  defects for a single-ion implantation has a peak value of 1300 at  $t=0.5$  ps and decreases rapidly with time, reaching a value of 750 at  $t=2$  ps. The peak value of  $n_b=6$  defects is 650 at  $t=1$  ps and 500 at  $t=2$  ps. For cluster ion impact, the number of  $n_b=5$  defects has a peak value, of approximately 1250 at  $t \sim 1$  ps for  $N_c=8$  and 20, and 2000 at  $t \sim 1$  ps for  $N_c=90$ , but decreases very gradually for all  $N_c$ . A number of  $n_b=6$  defects have a peak value of approximately 600 at  $t \sim 1$  ps and keeps their values at approximately  $t=2.5$  ps. A notable difference between the time dependence of the defect type for single-ion and cluster ion impacts is that the number of defects for  $n_b=3$  or  $n_b=7$  is very small for single-ion impact after 1 ps, while those for the cluster case remain 200 after 2 ps. These indicate that the defect nature induced by the impact in the two cases is different.

#### 4. Channeling of cluster implantation

First, we will examine the size dependence of the impact assuming that the cluster has purely translational velocity perpendicular to the surface, which means the internal veloc-

ity of the cluster is 0 K. In this case, all atoms are implanted without channeling. For  $N_c=20$  and 90, as can be seen in Fig. 5, the macroscopic upward expansion (or the vibration), which moves by a few nm, of the deformed region due to the impact prevents impurity atoms from going deeper by forcing them to move upward during the 3 ps after the impact. In the very early stage of the cluster impact, the atoms in the channeling site, which could go through the crystal region, are likely to collide with the lattice atoms in the cluster case, because the substrate atoms around the implanted atoms themselves move upward due to the macroscopic upward expansion. This phenomenon seems to be a reasonable explanation for reducing the channeling effect as compared with the mechanism proposed by Takeuchi *et al.*, where the amorphous layer automatically formed by the cluster impact reduces the channeling, since amorphization of the cluster impact is a much slower process than the channeling.

Decaborane experiments of Takeuchi *et al.* show channeling; i.e., one or two boron atoms in decaborane have enough energy to undergo channeling. The decaborane implantation may corresponds to our case of  $N_c=8$ , because the number of boron atoms in decaborane is 10. Since the mass of the boron is much smaller than the silicon, a boron cluster should be large to have a similar effect to that of the eight-silicon-cluster case. In our simulation, the character of implantation in the eight-silicon-cluster case is closer to that of single-ion implantation where the channeling occurs, because the cluster size of  $N_c=8$  is not large enough to make collective motions that prevent channeling as can be seen in Fig. 5. This explains why there is channeling in decaborane implantation. However, it is worth mentioning that we cannot deny the possibility that the smaller cluster dissociated from the melting cluster just before impact by the strong interaction between the cluster ion and the surface charge may cause channeling.

To reduce channeling the cluster size should be larger. We have shown that  $N_c=20$  is sufficiently large to prevent the channeling effect. So far we have studied the implantation by using the cluster having the purely translational velocity perpendicular to the surface. Here we study the effect of the inner state of the cluster on the impact: the cluster is injected as a melting form or the cluster is rotating. The melting case corresponds to the situation in which the decaborane is injected with melting, since its melting point is low (372.5 K). The rotating case accounts for the fact that the rotation of the cluster is most probable because it is difficult to control. To study the effects of these inner states of the cluster, we have also simulated additional 20-atom cluster impacts with various velocity conditions: (1) in which particles have random velocity with a far higher melting temperature (3000 K), and (2) in which particles move around the axis of the incident velocity. The corresponding energy of rotation is 4000 K. Note that these asymmetric properties of cluster impact are only attainable by the three-dimensional simulation performed here. In both cases and for  $N_c=20$ , however, a prominent channeling effect was not found as can be seen in Fig. 7. The deepest depth of impurity for the random (1) and rotational (2) velocity cases during the monitoring is 3.0 and 2.7 nm, both are close to that of the uniform velocity case, 2.9 nm. Truly, one of the cluster particles in the rotating cluster goes deeper into the surface compared

with other particles in the very early stages of the impact (0.1 ps after collision), but the particle collides with substrate atoms after 0.1 ps and cannot go deeper in our simulations. This tendency is unclear for the high-temperature melting case. Although the impurity distributions are very similar to one another for the three cases of  $N_c=20$ , the defect distribution is clearly different. See Fig. 8. The sharp protuberance in the defect distribution remain after 5 ps for the rotational cluster case, reflecting the impact of the asymmetric velocity distribution in the cluster. In these three cases, the fluctuation of the velocity of atoms in the cluster is not so high as compared to the translational velocity such that some of the atoms could not have sufficient energy to move to the interstitial states that lead to channeling. Thus additional fluctuation of the velocities or energies of the implanted atoms in the cluster  $N_c=20$  does not cause the channeling. This indicates that the  $N_c=20$  for silicon at about 5 keV may be sufficiently large to prevent the channeling. Because the mass of the boron is smaller than that of Si, larger clusters of boron or a lowering of the accelerating voltage of the ion implanter is necessary to achieve suppression of channeling in boron cluster implantation.

#### IV. CONCLUSION

In conclusion, we have simulated the collision of 5.7-keV silicon ion clusters of various sizes with a silicon substrate. We found that the damaged region of cluster implantation is shallower than the shallowest one for the single ion, although the deformed region near the surface becomes larger for the cluster case. With an increase in size (or the number of constituent atoms) of the cluster, we found that the damaged region becomes shallower. The change from the collision cascade that is a characteristic mechanism for single-ion implantation to the simultaneous collision process, which leads to the collective motion of particles such as macroscopic vibrations or shock waves, is found by increasing the size (number of the atoms) of the cluster. Our result shows that the impact energy for larger clusters is transferred partly by the shock wave or macroscopic vibrations, leading to suppression of the channeling effect. The small cluster ion implantation may suffer from the channeling, but it is clearly shown that the larger cluster suppress the inherent channeling overcoming the effect of the distribution of the velocities in the cluster. It is also found that the distribution of defects caused by the impact may deviate from the uniformity, reflecting the velocity fluctuations in the cluster if it is rotated.

Because a large amount of CPU time is required for performing molecular-dynamics simulations, the conclusions must be drawn from a single computer run or as representative of several runs. We hope that, in the future, parallel computing will make it easier to solve this statistical problem by performing simulations simultaneously on each processor node. Note, however, that since all atoms inside the cluster collide almost simultaneously with the substrate atoms, the results obtained from a single run for cluster implantation already has a statistical character compared with the single-ion case. Thus, in the cluster implantation case, the results for channeling where the peculiar trajectory of a impurity atom is important has less of a statistical character than those

for the defect and impurity distributions where many atoms are involved.

#### ACKNOWLEDGMENTS

We are grateful for the encouragement provided by Dr. Michiharu Nakamura and Shiroo Kamohara over the years.

We also thank Professor R. W. Dutton and Professor Bill Hoover for useful comments on the early stage of our work. We also thank Professor Richard Schlichting for his careful reading of the manuscript. One of the authors (S.I.) acknowledges the Real World Computing Partnership for support during the FY-1998, especially Dr. Jun'ichi Shimada for his useful advice.

- 
- <sup>1</sup>G. Kamarions and P. Felix, *J. Phys. D* **29**, 487 (1996).
- <sup>2</sup>For example boron diffusivity relates directly to the concentration of silicon self-interstitials, because the boron is thought to diffuse by an interstitialcy mechanism. Therefore the boron diffuses rapidly until the implant damage anneals out. See D. J. Eaglesham, P. A. Stolk, H.-J. Grossmann, and J. M. Poate, *Appl. Phys. Lett.* **65**, 2305 (1994).
- <sup>3</sup>S. Matsumoto (unpublished).
- <sup>4</sup>A. W. Kleyn, *Science* **275**, 1440 (1997).
- <sup>5</sup>For a general account of implantation, see for example, E. Rimini, *Ion Implantation: Basic to Device Fabrication* (Kluwer Academic, Boston, 1995).
- <sup>6</sup>T. Aoyama, K. Suzuki, H. Tashiro, Y. Toda, T. Yamazaki, K. Tasaki, and T. Ito, *J. Appl. Phys.* **77**, 417 (1995).
- <sup>7</sup>K. Goto, J. Matsuo, T. Sugii, H. Minakato, I. Yamada, and T. Hisatsugu, *Technical Digest of International Device Meeting, San Francisco, California* (IEEE, California, 1996), p. 435.
- <sup>8</sup>D. Takeuchi, N. Shimada, J. Matsuo, and I. Yamada, *Nucl. Instrum. Methods Phys. Res. B* **121**, 345 (1997).
- <sup>9</sup>*Atomic & Ion Collisions in Solids and at Surfaces*, edited by R. Smith (Cambridge University Press, Cambridge, 1997).
- <sup>10</sup>K. Nordlund, *Comput. Mater. Sci.* **3**, 448 (1995).
- <sup>11</sup>*Simulation of Liquids and Solids*, edited by G. Cicotti, D. Frenkel, and I. R. McDonald (Elsevier, Amsterdam, 1987).
- <sup>12</sup>W. G. Hoover, *Molecular Dynamics* (Springer-Verlag, Berlin, 1986); Wm. G. Hoover, *Computational Statistical Mechanics* (Elsevier, Amsterdam, 1991).
- <sup>13</sup>J. F. Ziegler, J. P. Biersack, and U. Littmark, *The Stopping and Range of Ions in Solids, The Stopping and Range of Ions in Matter*, edited by J. F. Ziegler (Pergamon, New York, 1985), Vol. 2.
- <sup>14</sup>K. M. Klein, C. Park, and Al F. Tash, *IEEE Trans. Electron Devices* **39**, 1614 (1992).
- <sup>15</sup>With imposing symmetry of crystal, Monte Carlo simulation can handle multiple scattering, such as A. I. Melker, in *Slow Positron Beam Techniques for Solids and Surfaces, 5th International Workshop*, edited by E. Ottewitte and A. H. Weiss, AIP Conf. Proc. 303 (AIP, New York, 1994), p. 151, but this applicability is rather limited as compared with molecular dynamics.
- <sup>16</sup>T. Díaz de la Rubia and G. H. Gilmer, *Phys. Rev. Lett.* **74**, 2507 (1995).
- <sup>17</sup>F. H. Stillinger and T. A. Weber, *Phys. Rev. B* **31**, 5262 (1985).
- <sup>18</sup>L. A. Marqués, M.-J. Caturla, T. Díaz de la Rubia, and G. H. Gilmer, *J. Appl. Phys.* **80**, 6160 (1996).
- <sup>19</sup>M.-J. Caturla, T. Díaz de la Rubia, L. A. Marqués, and G. H. Gilmer, *Phys. Rev. B* **54**, 16 683 (1996).
- <sup>20</sup>M. Jaraiz, G. H. Gilmer, D. M. Stock, and T. Díaz de la Rubia, *Nucl. Instrum. Methods Phys. Res. B* **102**, 180 (1995).
- <sup>21</sup>M. Jaraiz, G. H. Gilmer, J. M. Poate, and T. D. de la Rubia, *Appl. Phys. Lett.* **68**, 409 (1996).
- <sup>22</sup>Z. Insepov and I. Yamada, *Nucl. Instrum. Methods Phys. Res. B* **99**, 248 (1995).
- <sup>23</sup>Z. Insepov and I. Yamada, *Nucl. Instrum. Methods Phys. Res. B* **112**, 16 (1996).
- <sup>24</sup>G. H. Gilmer and C. Roland, *Radiat. Eff. Defects Solids* **130**, 321 (1994).
- <sup>25</sup>M. E. Barone and D. B. Graves, *J. Appl. Phys.* **78**, 6604 (1995).
- <sup>26</sup>W. E. Lorensen and H. E. Cline, *Comput. Graph.* **21**, 163 (1987).
- <sup>27</sup>ihara@crl.hitachi.co.jp
- <sup>28</sup>R. P. Webb and D. E. Harrison, Jr., *Appl. Phys. Lett.* **39**, 311 (1981). Shock wave propagation is observed in the global results for the statistical data obtained by simulation for single-ion implantation.
- <sup>29</sup>M.-O. Mewes, M. R. Andrews, D. M. Kurn, D. S. Durfee, C. G. Townsend, and W. Ketterle, *Phys. Rev. Lett.* **78**, 582 (1997).